Theoretical Prediction of the S_1-S_0 Internal Conversion of 6-Cyanoazulene

Yoshiaki Amatatsu*

Faculty of Engineering and Resource Science, Akita University, Tegata Gakuen-cho, Akita 010-8502, Japan

Received: February 8, 2007; In Final Form: April 12, 2007

Ab initio complete active-space self-consistent field (CASSCF) and second-order Multireference Möller−Plesset perturbation (MRMP2) calculations were performed to examine the S_1-S_0 internal conversion of 6-cyanoazulene (6CNAZ). The azulene skeletons of 6CNAZ in S_0 and S_1 have features that resemble those of azulene. The stable geometry in S_0 is characterized by (i) a C_{2v} structure, (ii) an aromatic bond-equalized structure in which all the peripheral skeletal bond distances resemble an aromatic CC bond distance, and (iii) a single bond character of the transannular bond. The stable geometry in S_1 is characterized by a nonaromatic C_{2v} structure. Contrary to similarities of the stable geometries in S_0 and S_1 between 6CNAZ and azulene, the conical intersection (S_1/S_0-CIX) of 6CNAZ is different from that of azulene. The S_1/S_0-CIX of 6CNAZ takes a planar structure, whereas that of azulene takes a nonplanar structure in the seven-membered ring (Amatatsu, Y.; Komura, K. *J. Chem. Phys.* **2006**, *125*, 174311/1−8). On the basis of those computational findings, we predict the photochemical behavior of 6CNAZ in the S_1-S_0 internal conversion.

1. Introduction

Azulene is well-known as a molecule that violates Kasha's rule: it is fluorescent from S_2, but substantially nonfluorescent from S_1. Since the first discovery of violation of Kasha's rule in 1955,[1] many experimental and theoretical approaches have been undertaken to clarify the abnormal photochemical behavior of azulene.[2] Nevertheless, a realistic picture of the S_1-S_0 internal conversion (IC) of azulene has not been presented because of a lack of information on the conical intersection (denoted by S_1/S_0-CIX hereafter), where the radiationless S_1-S_0 transition takes place. In 1996, Bearpark et al. first reported the S_1/S_0-CIX geometry to discuss the IC process.[3] Their S_1/S_0-CIX is characterized by the following: (i) it takes a planar structure with C_{2v} symmetry substantially, (ii) the bond-equalized structure in the peripheral CC skeleton, which is characteristic in S_0, disappears, and (iii) the transannular bond shrinks from a normal C−C single into a normal C═C double bond.

During the past decade, however, several new experimental findings have been reported:

(EXP1) The decay time of azulene in S_1 depends on excess energy in the electronic excitation of S_0-S_1: 1.7 ps for the vibrationless S_1 state and 0.4 ps for the excess energy of 1300 cm^{-1} above the S_1 electronic origin.[4] Similar results have been reported from other experiments.[5−9]

(EXP2) S_1/S_0-CIX is responsible for the ultrafast decay located 2000−2300 cm^{-1} above the S_1 electronic origin.[4,7,8]

(EXP3) Strong oscillatory signals attributable to low-frequency out-of-plane vibrations are observed before the decay,[4] although the contribution of the out-of-plane motion to the IC process has been indicated by other authors.[6−8]

Particularly EXP3 above seems to be beyond the theoretical description of Bearpark et al.: a new model is required. We reported a new conceptualization of S_1-S_0 IC of azulene, which enables us to explain the new experimental findings mentioned above.[10] The most important point among our computational findings is that S_1/S_0-CIX takes a nonplanar structure in the seven-membered ring related to the strong oscillations because of the out-of-plane low-frequency modes in the decay process of azulene in S_1.

To the best of our knowledge, however, no further experimental or computational findings support nonplanar S_1/S_0-CIXs of azulene or its derivatives. For that reason, we theoretically examined the effect on the S_1/S_0-CIX of 6-cyanoazulene (6CNAZ) to compare the S_1-S_0 IC of 6CNAZ with that of the parent azulene.

This paper is organized as follows. In the next section, we describe the calculation method. In section 3, we explain the electronic and geometrical structures of 6CNAZ at important conformations. Based on computational findings, we predict S_1-S_0 IC of 6CNAZ in comparison with that of azulene.

2. Method of Calculation

Complete active space self-consistent-field (CASSCF) calculations with 14 electrons in 14 orbitals (denoted as (14,14)-CASSCF) are desirable for quantitative discussion of the excited states of 6CNAZ because 6CNAZ has 14 π electrons that are originated from the azulene skeleton (10 π electrons) and the cyano group (4 π electrons). However, (14,14)CASSCF calculations are unrealistic to scan the potential energy surfaces for the S_1-S_0 IC of 6CNAZ. Consequently, to reduce the computational load, as we did for another system, diphenylacetylene,[11] we selected important π and π^* orbitals from all seven occupied π and the lowest seven π^* unoccupied orbitals to perform the configuration interaction (CI) method, where up to triple excitations from the closed-shell configuration are included (i.e., SDT−CI). Results showed that the occupation numbers of the lowest two π orbitals and those of the highest two π^* orbitals are respectively greater than 1.98 and less than 0.02, for all sampled conformations. Those results imply that the highest five π orbitals and the lowest five π^* orbitals are sufficient to describe S_0 and S_1 in our present interest. Therefore, we adopted (10,10)CASSCF method for the scan of the potential energy surfaces. At several conformations, we made corrections for

* Corresponding author. E-mail: amatatsu@ipc.akita-u.ac.jp. Fax: +81-18-889-2601. Phone: +81-18-889-2625.

10.1021/jp071092i CCC: $37.00
Published on Web 05/27/2007

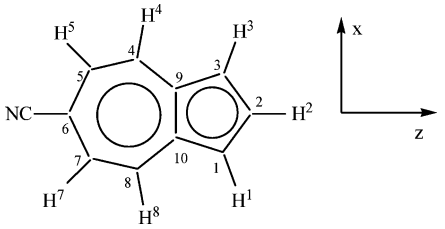

Figure 1. Numberings of atoms and definition of the coordinates of 6CNAZ. The *y*-axis is perpendicular to the *xz*-plane.

(10,10)CASSCF energy of each electronic state using second-order multireference Möller−Plesset perturbation (MRMP2). All valence and virtual orbitals were included in perturbation calculations. For this calculation, we imposed the constraint of C_s symmetry, as in the calculation of azulene[10] (see Figure 1). In other words, a planar structure of 6CNAZ is designed to have C_{2v} symmetry, but a nonplanar structure is allowed under the constraint of C_s symmetry. Appendix 1 is a detailed description of why the symmetry constraint was imposed.

First, we optimized the geometries in S_0 and S_1 for 6CNAZ (represented respectively as S_0-geometry and S_1-geometry). Then we optimized the conical intersection between S_1 and S_0 (S_1/S_0-CIX), where the radiationless relaxation takes place. To reduce computational labor in the optimization of S_1/S_0-CIX, we preformed a smaller (8,8)CASSCF calculation based on the preliminary CI result: at most, four occupied and four unoccupied π-type orbitals are sufficient to describe both S_0 and S_1 for the region where S_0 and S_1 are energetically similar. However, after optimization of S_1/S_0-CIX by (8,8)CASSCF, we performed a (10,10)CASSCF calculation at S_1/S_0-CIX and verified that the energy difference between S_1 and S_0 is sufficiently small to be a CIX. That fact implies that a much more computationally demanding (10,10)CASSCF gives an S_1/S_0-CIX similar to that by (8,8)CASSCF.

Electronically excited 6CNAZ at S_0-geometry travels into S_1/S_0-CIX in S_1 and then relaxes from S_1/S_0-CIX in S_0. One approach to investigate that phenomenon is to calculate the intrinsic reaction coordinate, as done previously in the case of the S_1-S_0 IC of azulene.[10] However, because the calculation of the intrinsic reaction coordinate is computationally demanding, we did three types of geometry optimization: (i) S_1-geometry optimization starting from S_0-geometry, (ii) that from S_1/S_0-CIX, and (iii) S_0-geometry optimization from S_1/S_0-CIX. Therefore, the geometries by optimizations i and ii become S_1-geometry and the geometry by optimization iii become S_0-geometry. Consequently, the reaction path is connected successively with three important conformations mentioned above. That is, after electronic excitation into S_1 at S_0-geometry, electronically excited 6CNAZ passes through S_1-geometry and reaches S_1/S_0-CIX. Then the non-adiabatic transition into S_0 takes place at S_1/S_0-CIX and finally reverts to S_0-geometry.

Except for the optimization of S_1/S_0-CIX by Gaussian 03,[12] we used the GAMESS program.[13] The basis set is Huzinaga−Dunning double-ζ (DZ) quality; polarization functions are added on the carbon atoms ($\alpha_d = 0.75$) for the azulene skeleton and the nitrogen atom ($\alpha_d = 0.80$) (i.e., DZP quality). As described in Appendix 2, the addition of polarization functions on the carbon atoms of the azulene skeleton is necessary to obtain a reasonable S_1/S_0-CIX of azulene and its derivatives.

3. Results

3.1. Geometries. We preface results with a comment on the 6CNAZ geometrical features. Table 1 presents the optimized parameters for three important conformations (i.e., S_0-geometry, S_1-geometry, and S_1/S_0-CIX) of 6CNAZ, along with those of the parent molecule of azulene. Regarding S_0-geometry, the geometrical feature of the azulene skeleton resembles that of azulene. All peripheral CC bond distances are similar to an aromatic CC bond distance. The transannular C^9C^{10} bond has an almost single CC bond character. Dihedral angles shown in Table 1 indicate that S_0-geometry has a planar structure with C_{2v} symmetry. Therefore, we call S_0-geometry an aromatic bond-equivalent structure.

TABLE 1: Characteristic Optimized Parameters of 6CNAZ and Azulene[a]

	S_0-geometry	S_1-geometry	S_1/S_0-CIX
	Bond Distances (Å)		
C^2C^3	1.395 (1.410)[b]	1.387 (1.405)	1.380 (1.401)
C^3C^9	1.408 (1.408)	1.467 (1.464)	1.517 (1.498)
C^9C^4	1.391 (1.396)	1.447 (1.445)	1.495 (1.487)
C^4C^5	1.403 (1.404)	1.380 (1.387)	1.359 (1.332)
C^5C^6	1.407 (1.404)	1.433 (1.424)	1.455 (1.462)
C^9C^{10}	1.500 (1.498)	1.380 (1.390)	1.315 (1.359)
C^6C	1.457	1.448	1.440
CN	1.151	1.152	1.142
	Bond Angles (deg)		
$<C^1C^2C^3$	110.3 (109.6)	107.5 (107.0)	106.3 (106.9)
$<C^2C^3C^9$	108.6 (108.6)	109.3 (109.2)	109.7 (109.2)
$<C^3C^9C^{10}$	106.3 (106.6)	107.0 (107.3)	107.1 (107.3)
$<C^4C^9C^{10}$	127.7 (127.7)	129.5 (129.4)	130.6 (128.9)
$<C^5C^4C^9$	128.9 (128.6)	127.2 (126.8)	125.9 (125.3)
$<C^6C^5C^4$	128.6 (128.8)	129.0 (129.5)	129.3 (128.7)
$<C^7C^6C^5$	129.7 (129.7)	128.7 (128.6)	128.5 (125.4)
	Torsional Angles (deg)		
$<C^1C^2C^3C^9$	0.0 (0.0)	0.0 (0.0)	−0.0 (−0.6)
$<C^2C^3C^9C^{10}$	0.0 (0.0)	0.0 (0.0)	0.0 (0.4)
$<C^5C^4C^9C^{10}$	0.0 (0.0)	0.0 (0.0)	0.1 (19.4)
$<C^6C^5C^4C^9$	0.0 (0.0)	0.0 (0.0)	−0.0 (−3.2)
$<C^7C^6C^5C^4$	0.0 (0.0)	0.0 (0.0)	−0.1 (−26.6)

[a] Because of a constraint of C_s symmetry, the bond distance of C^2C^1, for instance, is identical to that of C^2C^3. Similarly, the bond angle of $C^2C^1C^{10}$ is identical to that of $C^2C^3C^9$. The dihedral angle of $C^{10}C^1C^2C^3$ is identical to that of $C^9C^3C^2C^1$ with an opposite sign. [b] Values in the parentheses are optimized parameters of azulene, taken from ref 10.

Geometrical features of S_1-geometry are also similar to those of azulene. The S_1-geometry has a planar structure with C_{2v} symmetry as does the S_0-geometry (see the relevant dihedral angles in Table 1). However, the skeletal bond distances differ greatly from those at S_0-geometry. The 6CNAZ at S_1-geometry loses the aromatic bond-equivalent character of S_0-geometry. The transannular C^9C^{10} bond greatly increases the double bond character. Concomitant with the shrinkage of the transannular bond, the peripheral CC bond distances change considerably: C^3C^9 and C^9C^4 (also C^1C^{10} and $C^{10}C^8$ because of the constraint of C_s symmetry) that are bonded to the transannular C^9C^{10} bond lengthen. In fact, C^4C^5 shrinks and C^5C^6 lengthens.

The skeletal bond distances at S_1/S_0-CIX of 6CNAZ are also similar to that of azulene. The skeletal feature of S_1-geometry is enhanced at S_1/S_0-CIX: the C^3C^9, C^4C^9, and C^5C^6 bonds become longer than those at S_1-geometry, although the C^4C^5 and C^9C^{10} bonds become shorter. In contrast to the similarities of the skeletal bond distances between 6CNAZ and azulene, the dihedral angles differ greatly from those of azulene. Table 1 shows that the seven-membered ring of 6CNAZ has a planar structure, whereas that of azulene has a nonplanar structure.

3.2. Electronic Structures. This subsection presents discussion of electronic structures in relation to the geometrical features described above. Table 2 shows the electronic structures at S_0-geometry. The S_1 state is well described using the highest occupied molecular orbital−lowest unoccupied molecular orbital

TABLE 2: Electronic Structures of 6CNAZ at S_0-Geometry

		dipole moment (Debye)[a]		
	energy (eV)	μ_z	μ_y	main CSFs[b]
S_0	0.0 (0.0)[c]	3.805	0.0	0.875 (closed shell)
S_1	2.077 (1.713)	5.003	0.0	0.843 (1−1′)

[a] The *z*- and *y*-directions are defined in Figure 1. [b] The CSFs of which absolute values of CASSCF coefficients are greater than 0.3 are listed. The five occupied π-orbitals and the lowest five unoccupied π*-orbitals in the order of energy are designated, respectively, as 5, 4, 3, 2, 1(HOMO), 1′(LUMO), 2′, 3′, 4′, and 5′; 1−1′ in the parenthesis, for instance, indicates the CSF of single excitation from orbital 1 to 1′. [c] Values in the parentheses are those by MRMP2.

TABLE 3: Electronic Structures of 6CNAZ at S_1/S_0-CIX

		dipole moment (Debye)[a]		
	energy (eV)[b]	μ_z	μ_y	main CSFs[c]
S_0	1.838 (1.366)[d]	2.532	−0.005	0.775 (closed shell) + 0.350 (2−1)
S_1	1.844 (1.495)	4.768	−0.004	0.836 (1−1)

[a] Because of the nonplanarity at S_1/S_0-CIX, the *z*- and *y*-directions are different from the original space-fixed coordinate in Figure 1. By diagonalizing the tensor of the moment of inertia, we determined the new *z*- and *y*-directions. The new *z*- and *y*-components of the moment of inertia correspond, respectively, to the smallest and the largest components. [b] The energy is relative to that in S_0 at S_0-geometry. [c] The CSFs, of which the absolute values of CASSCF coefficients are greater than 0.3, are listed. The five occupied π-orbitals and the lowest five unoccupied π*-orbitals in the order of energy are designated, respectively, as 5, 4, 3, 2, 1(HOMO), 1′(LUMO), 2′, 3′, 4′, and 5′; 1−1′ in the parenthesis, for instance, indicates the CSF of single excitation from orbital 1 to 1′. [d] Values in parentheses are those by MRMP2.

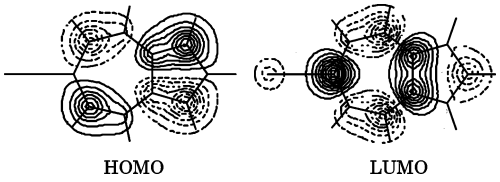

Figure 2. HOMO and LUMO at S_0-geometry.

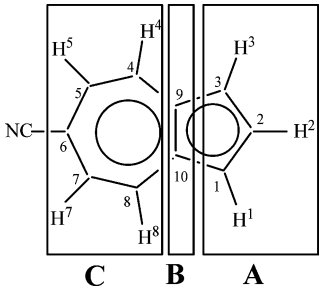

Figure 3. 6CNAZ divided into fragments.

(HOMO−LUMO) single excitation. Figure 2 shows that the character of molecular orbitals (MOs) in the transannular C^9C^{10} part changes from an antibonding (in HOMO) orbital into a bonding (in LUMO) orbital, which engenders shrinkage of the transannular bond in S_1. The changes of the peripheral CC bonds in S_1 can also be related to changes of the MO nature in relevant parts.

Table 3 lists the electronic structure at S_1/S_0-CIX using (10,-10)CASSCF. The energy difference (0.006 eV) is sufficiently small to be a CIX, which implies that S_1/S_0-CIX by (8,8)-CASSCF described above is similar to S_1/S_0-CIX by (10,10)-CASSCF which is impractical because of an extremely large computational load. The main configuration state functions (CSFs) indicate that S_0 and S_1 are well described, respectively, by the closed-shell CSF and the HOMO−LUMO single excitation, which is similar to the case for electronic structures at S_0-geometry (see Table 2) and those of S_1-geometry.

3.3. Dipole Moments. The dipole moments and charge populations are useful to deepen understanding of the 6CNAZ photochemical process. Table 4 presents dipole moments and the charge populations at important conformations along with those of azulene. Figure 3 shows the definition of each fragment for the charge population. The change of the dipole moments of 6CNAZ (1.198 D) at S_0-geometry resembles that of azulene (1.004 D) because some charge in fragment A transfers to the remaining parts (especially fragment C) through electronic excitation into S_1 in cases of 6CNAZ and azulene.

The dipole moment for S_1-geometry resembles that for S_0-geometry. However, the charge population in each fragment changes; some charges in A and C move into the transannular part B, which is related to the geometrical change by which the transannular C^9C^{10} bond increases its double bond character during the process of S_0-geometry → S_1-geometry in S_1. The charge transfer into B continues, reflecting the increasing double-bond character of the transannular C^9C^{10} bond during the process of S_1-geometry → S_1/S_0-CIX. A similar discussion can also be made for the case of the S_1-geometry → S_1/S_0-CIX process of azulene, as far as the charge in B is concerned (Table 4). Nevertheless, S_1/S_0-CIX of 6CNAZ differs greatly from that of azulene; the former takes a planar structure in the seven-membered ring, whereas the latter is nonplanar. The charge population of fragment C in S_1 can explain this geometrical difference. As Table 4 shows, the charge population in C is much less negative than that of azulene. Therefore, the structure around the C^6 atom of 6CNAZ resembles a planar carbocation, whereas that of azulene resembles a nonplanar carbanion.

At S_1/S_0-CIX, the dipole moment in S_1 (long-axis component; 4.768 D) changes suddenly into that in S_0 (2.532 D), which differs greatly from that for S_0-geometry. The decrease of the dipole moment (2.236 D) is comparable to that of azulene (long axis component; 1.733 D). Therefore, the large difference of the S_0 dipole moment between S_1/S_0-CIX and S_0-geometry is ascribed to the fact that the nonaromatic azulene skeleton at S_1/S_0-CIX is very different from the aromatic one for S_0-geometry.

Summarizing the role of the cyano group in the S_1–S_0 IC of 6CNAZ, Table 4 shows that the charge population in the cyano group is almost constant, irrespective of the conformation or electronic state. Furthermore, the CN and C^6C bond distances remain almost unchanged, as shown in Table 1. Therefore, the electron-withdrawing capability of the cyano group is almost constant in all S_1-S_0 IC processes, which is related to the fact that many similarities are apparent in the computational findings between 6CNAZ and the parent azulene, as described above. The electron-withdrawing capability of the cyano group produces an interesting difference at S_1/S_0-CIX: the planar seven-membered ring for 6CNAZ and the nonplanar one for azulene.

3.4. Prediction of S_1-S_0 IC Process. To predict the S_1-S_0 IC of 6CNAZ, we briefly review the previously reported picture of azulene.[10] Figure 4a shows that the S_1-S_0 IC process of azulene schematically. Upon excitation into S_1 at aromatic bond-equivalent S_0-geometry, azulene is skeletally relaxed into a planar but nonaromatic S_1-geometry. After passing through the region around S_1-geometry, a nonplanarity in the seven-membered ring becomes important so that azulene reaches S_1/S_0-CIX. The energetic instability in the process of S_1-geometry → S_1/S_0-CIX (0.426 eV in Table 5) is comparable to the

TABLE 4: Dipole Moment Components and Mulliken Charges of 6CNAZ and Azulene

		dipole moment (Debye)[a]		Mulliken charge[b]			
geometry	state	μ_z	μ_y	A	B	C	CN
			6-CNAZ				
S_0-geometry	S_0	3.805	0.0	−0.31	0.55	−0.08 (0.25)[c]	−0.16
	S_1	5.003	0.0	−0.21	0.52	−0.13 (0.22)	−0.18
S_1-geometry	S_1	4.935	0.0	−0.17	0.41	−0.07 (0.18)	−0.17
S_1/S_0-CIX	S_1	4.768	−0.004	−0.14	0.32	−0.03 (0.15)	−0.16
	S_0	2.532	−0.005	−0.25	0.30	0.09 (0.18)	−0.14
			Azulene[d]				
S_0-geometry	S_0	−0.715[e]	0.0	−0.32	0.52	−0.38[f] (−0.15)[c]	(0.18)[g]
	S_1	0.289	0.0	−0.24	0.51	−0.46 (−0.20)	(0.18)
S_1-geometry	S_1	0.253	0.0	−0.19	0.40	−0.39 (−0.23)	(0.18)
S_1/S_0-CIX	S_1	0.075	−0.136	−0.16	0.29	−0.32 (−0.26)	(0.18)
	S_0	−1.658	−0.146	−0.26	0.28	−0.21 (−0.22)	(0.19)

[a] The *z*- and *y*-directions are determined similarly to those shown in Table 3. [b] Fragments A, B, and C are defined in Figure 3. [c] Values in parentheses are the charges on the C^6 atom. [d] Values of azulene are taken from ref 10. [e] The signs of μ_z are opposite those in ref 10 because the *z*-direction in Figure 1 is opposite that of ref 10. [f] Values are different from those in ref 10 because fragment C does not include the H^6 atom bonded to the C^6 atom in the definition of Figure 3. [g] Values in parentheses are the charges on the H^6 atom for azulene.

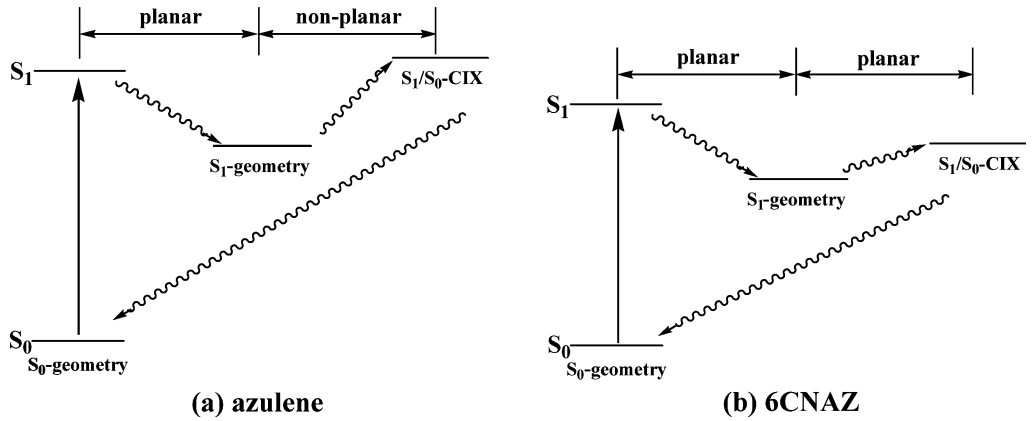

Figure 4. Schematic representation of S_1-S_0 internal conversion of (a) azulene and (b) 6CNAZ.

TABLE 5: Energies of 6CNAZ and Azulene

geometry	S_0	S_1
	6CNAZ[a]	
S_0-geometry	0.0	2.077 (1.713)
S_1-geometry	0.618 (0.487)	1.549 (1.390)
S_1/S_0-CIX	1.838 (1.366)	1.844 (1.495)
	Azulene[b]	
S_0-geometry	0.0	1.952
S_1-geometry		1.556
S_1/S_0-CIX	1.803	1.982

[a] Values in the parentheses are those by MRMP2. [b] The values are taken from ref 10.

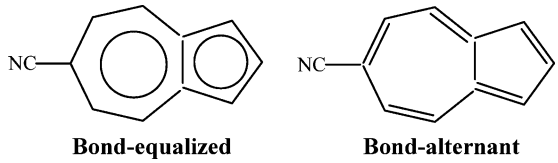

Figure A1. Aromatic bond-equalized structure and nonaromatic bond-alternant structure of 6CNAZ.

energetic stability between S_0-geometry and S_1-geometry (0.396 eV). These computational findings can be related to the experimental findings EXP1 to EXP3 described in the Introduction. During the stay in S_1, azulene is subjected to a large geometrical change from S_0-geometry into S_1/S_0-CIX. The period of the stay in S_1 corresponds to the experimental decay time (1−2 ps) (4−9). The excess energy of 1000−1300 cm^{-1} above the S_1 origin drastically decreases the lifetime (ca. 0.4 ps) or broadening of the rotational line width.[4,8] In this region, several totally symmetric in-plane (i.e., a_1-type under C_{2v}) vibrations exist. One vibrationally excited-state in S_1 can facilitate azulene's change from S_0-geometry into S_1-geometry. Therefore, azulene with excess energy of 1000−1300 cm^{-1} in S_1 can pass over S_1-geometry and reach S_1/S_0-CIX more effectively. Two computational findings related to the process of S_1-geometry → S_1/S_0-CIX, i.e., the nonplanarity of the seven-membered ring and the energetic instability, can be related to the experimental observation of strong oscillations because of the out-of-plane motions that occur before the decay.[4] To reach S_1/S_0-CIX from S_0-geometry in S_1, the out-of-plane motion in the seven-membered ring is necessary, but it does not play an important role until electronically excited azulene passes over the most stable geometry in S_1 (i.e., S_1-geometry). In other words, the out-of-plane motion in the seven-membered ring is promoted on the impulsive S_1 potential energy surface between S_1-geometry and S_1/S_0-CIX. Therefore, any out-of-plane vibration is inactive in the S_0-S_1 electronic transition; nevertheless, the strong oscillation of the out-of-plane mode occurs before the decay.

Now we predict the S_1-S_0 IC of 6CNAZ. As presented in Table 5, the energetic stability in the process of S_0-geometry → S_1-geometry in S_1 (0.528 eV) is similar to that of azulene, whereas the energetic instability of S_1-geometry → S_1/S_0-CIX (0.295 eV) is much smaller. As for azulene, 6CNAZ is subject to a similar large skeletal change in the process of S_0-geometry → S_1/S_0-CIX. Therefore, we predict that the lifetime in S_1 of 6CNAZ is shorter than that of azulene in equivalent experimental conditions. Furthermore, using vibrational analysis at

S_0-geometry, we found that several totally symmetric in-plane vibrations exist in the region of 1000−1300 cm^{-1}. Therefore, the excess energy of 1000−1300 cm^{-1}, which serves 6CNAZ to deform from aromatic S_0-geometry into nonaromatic S_1-geometry, is likely to shortening the decay time drastically, as found in case of azulene. Finally, we predict oscillatory signals because the out-of-plane vibrations are slight or nonexistent in the decay of 6CNAZ, which can be explained as (i) a planar structure at S_1/S_0-CIX or (ii) slight energetic instability in the process of S_1-geometry $\rightarrow S_1/S_0$-CIX.

Before terminating the prediction of the S_1–S_0 IC of 6CNAZ, we examine the reliability of the present discussion based on the CASSCF results. Table 5 shows that the MRMP2 energetic corrections are not so different from each other, irrespective of conformations and electronic states. For that reason, the above discussion based on the CASSCF results will change greatly by use of a more sophisticated MRMP2 method. It is expected that the MRMP2 discussion on the S_1-S_0 IC of 6CNAZ would be changed because the global potential energy surfaces are commonly shifted-down by ca. 0.3 eV. In Figure 4b, we show a schematic representation of the S_1–S_0 IC of 6CNAZ, in which the MRMP2 effect is considered.

4. Concluding Remarks

In this study, we predicted the S_1-S_0 IC of 6CNAZ in comparison with that of azulene. Results show that many similarities of the geometries and the electronic states exist between 6CNAZ and azulene. At the stable geometry in S_0, all peripheral bonds are similar to a CC bond distance of aromatic benzene; furthermore, the transannular bond resembles a CC single bond. Upon electronic excitation into S_1, however, the aromaticity is lost, and the transannular bond greatly increases its double bond character so that 6CNAZ is skeletally relaxed with a planar structure in S_1. In addition, S_1/S_0-CIX of 6CNAZ contrasts to that of azulene. The former almost retains its planar structure in the seven-membered ring and does not become energetically unstable to a great degree relative to the stable geometry in S_1 (i.e., S_1-geometry). The latter takes a nonplanar conformation and becomes unstable relative to S_1-geometry. The electron-withdrawing cyano group plays an important role in creating a planar structure at S_1/S_0-CIX. On the basis of these computational findings, we were able to predict the experimental findings for S_1-S_0 IC of 6CNAZ:

i) The excess energy of 1000−1300 cm^{-1} above the S_1 origin drastically decreases the lifetime in S_1, as observed also in case of azulene.

ii) The lifetime in S_1 is likely to be shorter than that of azulene because the energetic location of S_1/S_0-CIX relative to the S_1 state is lower than that of azulene.

iii) In contrast to the case of azulene, little or no oscillatory signal attributable to the low-frequency out-of-plane motions is expected.

To verify our predictions of the S_1–S_0 IC of 6CNAZ and to justify our interpretation on that of azulene, we hope to use an experimental approach on the photochemistry of 6CNAZ.

Appendix 1

As clarified previously,[10,14] the stable geometry of azulene in S_0 is strongly dependent on its computational method. We investigated whether the stable geometry of 6CNAZ in S_0 (S_0-geometry) is dependent on the computational method. Two possible conformations of S_0-geometry (Figure A1) exist: an aromatic bond-equalized conformation in which all peripheral CC bonds are similar to an aromatic CC bond; and a bond-alternant conformation, by which a peripheral CC skeleton alternates the C═C double bond with the C−C single bond. In Table A1, we listed the optimized skeletal bonds with our present basis set described in section 2. Although the stable geometry in S_0 has a planar structure in any computational method, only the second-order Möller−Plesset perturbation (MP2) method gives a bond-equivalent structure (i.e., C_{2v} geometry); the other methods give a bond-alternant structure (i.e., C_s geometry). We then performed a CASSCF optimization under constraint of C_{2v} symmetry. As presented in Table A1, the optimized geometry under C_{2v} constraint yields a similar result to that using MP2 method. At the C_s and C_{2v} CASSCF geometries, we made energetic Multireference MP2 (MRMP2) corrections. The C_{2v} geometry (i.e., aromatic bond-equalized structure) is more stable by 0.554 eV than the C_s geometry (bond-alternant structure) with MRMP2 correction, although it is unstable by 0.870 eV without MRMP2 correction (i.e., only CASSCF). On the basis of these computational findings, we must impose a C_{2v} symmetry constraint to obtain a reasonable bond-equalized structure in S_0 by the present (10,10) CASSCF method. However, 6CNAZ can take a nonplanar structure, especially at S_1/S_0-CIX, as indicated in the text. We loosened the geometrical constraint from C_{2v} into C_s symmetry, in which the *yz*-plane in Figure 1 is a symmetry plane.

We also examined whether geometries in S_1 are frustrated under the constraint of C_s symmetry of the *yz*-plane. We performed vibrational analyses at several conformations with C_s symmetry ranging from S_0-geometry to S_1/S_0-CIX. Results showed no imaginary frequency in S_1 for any conformation, although only one imaginary frequency in S_0 exists for each conformation (e.g., 416*i* cm^{-1} at S_0-geometry) leading to a bond-alternate structure. For that reason, the S_1 state is destabilized by a vibration leading to a bond-alternant structure, irrespective of conformations, whereas the S_0 state is stabilized incorrectly at the level of CASSCF calculation. This is identical to the case of azulene.[10] Therefore, we can say that the C_s symmetry constraint of *yz*-plane serves to give a more reasonable structure in S_0 than in either S_1 or S_0. Considering these computational findings, it seems natural that S_1/S_0-CIX has C_s symmetry of the *yz*-plane. Actually, we performed an S_1/S_0-CIX optimization

TABLE A1: Dependency of the Stable Geometry in S_0 on Computational Method

method	RHF	(10,10)CASSCF	(10,10)CASSCF/C_{2v}[a]	MP2
		Bond Distances (Å)[b]		
C^2C^3	1.441 (1.361)	1.469 (1.342)	1.395	1.414 (1.414)
C^3C^9	1.363 (1.439)	1.367 (1.466)	1.408	1.410 (1.410)
C^9C^4	1.426 (1.355)	1.444 (1.357)	1.391	1.397 (1.397)
C^4C^5	1.356 (1.430)	1.359 (1.457)	1.403	1.404 (1.404)
C^5C^6	1.439 (1.362)	1.467 (1.345)	1.407	1.415 (1.415)
C^9C^{10}	1.489	1.486	1.500	1.504

[a] The geometry was optimized under constraint of C_{2v} symmetry. [b] The numbers in the parentheses are the corresponding bond distances in the *yz*-plane in Figure 1.

TABLE A2: Basis set Dependency of S_1/S_0-CIX of Azulene

method/basis set	(8,8)CASSCF/ DZP[a]	(8,8)CASSCF(C_{2v})/ DZP[a,b]	(8,8)CASSCF/ DZ
	Bond Distances (Å)		
C^2C^3	1.401	1.399	1.410
C^3C^9	1.498	1.529	1.508
C^9C^4	1.487	1.527	1.489
C^4C^5	1.332	1.318	1.387
C^5C^6	1.462	1.472	1.439
C^9C^{10}	1.359	1.317	1.321
	Bond Angles (deg)		
$<C^1C^2C^3$	106.9	106.1	106.0
$<C^2C^3C^9$	109.2	109.5	109.0
$<C^3C^9C^{10}$	107.3	107.5	108.0
$<C^4C^9C^{10}$	128.9	130.2	130.4
$<C^5C^4C^9$	125.3	125.5	125.8
$<C^6C^5C^4$	128.7	130.8	129.8
$<C^7C^6C^5$	125.4	127.0	128.1
	Torsional Angles (deg)		
$<C^1C^2C^3C^9$	−0.6	0.0	0.0
$<C^2C^3C^9C^{10}$	0.4	0.0	−0.0
$<C^5C^4C^9C^{10}$	19.4	0.0	0.1
$<C^6C^5C^4C^9$	−3.2	0.0	−0.0
$<C^7C^6C^5C^4$	−26.6	0.0	−0.0

[a] The values are taken from ref 10, but the numberings of atoms are changed according to the present ones. [b] The geometry was optimized under constraint of C_{2v} symmetry.

without any symmetry constraint to obtain the same S_1/S_0-CIX. For those reasons, our present calculation, in which the C_s symmetry constraint is imposed, is proper to obtain reasonable structures and to reduce the computational load.

Appendix 2

As clarified in our previous paper,[10] S_1/S_0-CIX has a nonplanar structure in the seven-membered ring, whereas S_1/S_0-CIX by Bearpark et al. has a substantially planar structure.[3] To examine their differences, we performed an additional S_1/S_0-CIX optimization of the parent molecule of azulene using (8,8) CASSCF with a double-ζ (DZ) basis set; the active space is identical, but the polarization functions on the carbon atoms of the azulene skeleton are removed. Table A2 portrays S_1/S_0-CIX using three computation types. Apparently, S_1/S_0-CIX without polarization functions (i.e., DZ quality) tends to take a planar structure. In other words, the polarization functions on the carbon atoms of the azulene skeleton (i.e., DZP) are important to ensure the flexibility of S_1/S_0-CIX. In the present computation of 6CNAZ, S_1/S_0-CIX takes a planar structure even by addition of the polarization functions on the azulene skeleton, which implies that a planar S_1/S_0-CIX of 6CNAZ and a nonplanar S_1/S_0-CIX of azulene are realistic conformations.

Acknowledgment. Numerical calculations were performed partly at the Computer Center of Institute for Molecular Science. This work was financially supported by a Grant-in-Aid for Scientific Research (C) (No. 18550005) from the Ministry of Education, Culture, Sports, Science and Technology.

Supporting Information Available: All Cartesian coordinates at the important conformations mentioned in Section 3.1 are available free of charge via the Internet at http://pubs.acs.org.

References and Notes

(1) Beer, M.; Longuet-Higgins, H. C. *J. Chem. Phys.* **1955**, *23*, 1390−1391.

(2) See ref 10 for a more detailed review of the experimental and theoretical studies.

(3) Bearpark, M. J.; Bernardi, F.; Clifford, S.; Olivucci, M.; Robb, M. A.; Smith, B. R.; Vreven, T. *J. Am. Chem. Soc.* **1996**, *118*, 169−175.

(4) Wurzer, A. J.; Wilhelm, T.; Piel, J.; Reidle, E. *Chem. Phys. Lett.* **1999**, *299*, 296−302.

(5) Amirav, A.; Jortner, J. *J. Chem. Phys.* **1984**, *81*, 4200−4205.

(6) Suzuki, T.; Ito, M. *J. Phys. Chem.* **1987**, *91*, 3537−3542.

(7) Wagner, B. D.; Szymanski, M.; Steer, R. O. *J. Chem. Phys.* **1993**, *98*, 301−307.

(8) Ruth, A. A.; Kim, R.-K.; Hese, A. *Phys. Chem. Chem. Phys*. **1999**, *1*, 5121−5128.

(9) Foggi, P.; Neuwahl, F. V. R.; Moroni, L.; Salvi, P. R. *J. Phys. Chem. A* **2003**, *107*, 1689−1696.

(10) Amatatsu, Y.; Komura, Y. *J. Chem. Phys.* **2006**, *125*, 174311/1−8.

(11) Amatatsu, Y.; Hosokawa, M. *J. Phys. Chem. A* **2004**, *108*, 10238−10244.

(12) Frisch, M. J.; Trucks, G. W.; Schlegel, H. B.; Scuseria, G. E.; Robb, M. A.; Cheeseman, J. R.; Montgomery, Jr., J. A.; Vreven, T.; Kudin, K. N.; Burant, J. C.; Millam, J. M.; Iyengar, S. S.; Tomasi, J.; Barone, V.; Mennucci, B.; Cossi, M.; Scalmani, G.; Rega, N.; Petersson, G. A.; Nakatsuji, H.; Hada, M.; Ehara, M.; Toyota, K.; Fukuda, R.; Hasegawa, J.; Ishida, M.; Nakajima, T.; Honda, Y.; Kitao, O.; Nakai, H.; Klene, M.; Li, X.; Knox, J. E.; Hratchian, H. P.; Cross, J. B.; Adamo, C.; Jaramillo, J.; Gomperts, R.; Stratmann, R. E.; Yazyev, O.; Austin, A. J.; Cammi, R.; Pomelli, C.; Ochterski, J. W.; Ayala, P. Y.; Morokuma, K.; Voth, G. A.; Salvador, P.; Dannenberg, J. J.; Zakrzewski, V. G.; Dapprich, S.; Daniels, A. D.; Strain, M. C.; Farkas, O.; Malick, D. K.; Rabuck, A. D.; Raghavachari, K.; Foresman, J. B.; Ortiz, J. V.; Cui, Q.; Baboul, A. G.; Clifford, S.; Cioslowski, J.; Stefanov, B. B.; Liu, G.; Liashenko, A.; Piskorz, P.; Komaromi, I.; Martin, R. L.; Fox, D. J.; Keith, T.; Al-Laham, M. A.; Peng, C. Y.; Nanayakkara, A.; Challacombe, M.; Gill, P. M. W.; Johnson, B.; Chen, W.; Wong, M. W.; Gonzalez, C.; Pople, J. A. *Gaussian 03*, Revision B.04; Gaussian, Inc.: Pittsburgh, PA, 2003.

(13) Schmidt, M. W.; Baldridge, K. K.; Boatz, J. A.; Elbert, S. T.; Gordon, M. S.; Jensen, J. H.; Koseki, S.; Matsunaga, N.; Nguyen, K. A.; Su, S. J.; Windus, T. L.; Dupuis, M.; Montgomery, Jr., J. A. *J. Comput. Chem.* **1993**, *14*, 1347−1363.

(14) Kozlowski, P. M.; Rauhut, G.; Pulay, P. *J. Chem. Phys.* **1995**, *103*, 5650−5661.